




Characterization of CTBT-Relevant Radioxenon Detections at IMS Stations Using Isotopic Activity Ratio Analysis

BOXUE LIU,¹  MARTIN KALINOWSKI,¹ YUNWEI SUN,² CHARLES R. CARRIGAN,^{2,3} CHRISTOS SARAGIOTIS,¹ JUN WANG,¹ MARTIN ERTL,¹ YUICHI KIJIMA,¹ ROBIN SCHOEMAKER,¹ JOLANTA KUŚMIERCZYK-MICHULEC,¹ ANNE TIPKA,¹ and TARABAY ANTOUN²

Abstract—Radioxenon isotopes measured at radionuclide stations of the Comprehensive Nuclear-Test-Ban Treaty's (CTBT) International Monitoring System (IMS) may indicate releases from underground nuclear explosions (UNEs) but are often caused by emissions from nuclear facilities. Characterization of CTBT-relevant nuclear events may use the evolution of isotopic activity ratios over time, which goes from the release of an assumed UNE, through atmospheric transport, to sample collections and measurements. A mathematical approach is presented to discuss the characterization of the spatial and temporal relationships between a nuclear explosion and radioxenon measurements. On the one hand, activity concentrations at an IMS station are estimated by using the assumed release scenario regarding a UNE and atmospheric transport modelling. On the other hand, the activities collected in the samples are determined by spectral analysis first and the activity concentrations in the air passing over the IMS station are estimated under an assumption of constant concentration during sampling. The isotopic ratios of activities released from the UNE are related to the isotopic ratios of activity concentrations in the plume of air crossing the IMS station, resulting in a function of the isotopic activity ratio over the time from detonation to sample measurement. The latter is used for discrimination of a nuclear test and estimation of the time of detonation, such as a four radioxenon plot of the activity ratio relationship of $^{135}\text{Xe}/^{133}\text{Xe}$ versus $^{133\text{m}}\text{Xe}/^{131\text{m}}\text{Xe}$.

Keywords: Underground nuclear explosion, radioxenon, isotopic activity ratio, atmospheric transport modelling, international monitoring system, CTBT.

1. Introduction

Activity ratios of Comprehensive Nuclear-Test-Ban Treaty (CTBT) relevant radionuclides detected in particulate and noble gas samples can be used to discriminate a nuclear explosion source against the releases originating from other nuclear facilities. In case all four radioxenon isotopes are detected, the most discriminating plot is the activity ratio relationship between $^{133\text{m}}\text{Xe}/^{131\text{m}}\text{Xe}$ and $^{135}\text{Xe}/^{133}\text{Xe}$. An important feature is that observation data can be mapped onto the chart for distinguishing underground nuclear explosions (UNEs) from civilian applications without knowing the detonation time. This approach can only be applied to an early release, e.g., less than a few days, due to a short half-life of ^{135}Xe (9.14 h). For all combinations of isotopes with ^{135}Xe in the numerator it takes less than five days before the non-fractionated release from a nuclear explosion reaches the chemical equilibrium (Kalinowski, 2011; Kalinowski & Pistner, 2006; Kalinowski et al., 2010).

The activity ratios of two radioxenon isotopes detected routinely at IMS stations, such as $^{133}\text{Xe}/^{131\text{m}}\text{Xe}$, are typically found in a range which might originate from nuclear facilities such as medical isotope production facilities or from a delayed release of a nuclear test (Kalinowski & Liu, 2020). For example, the activity ratios of $^{133}\text{Xe}/^{131\text{m}}\text{Xe}$ recorded in April 2013 are considered strong evidence for the nuclear nature of a seismic event on 12 February 2013 related to an announced DPRK nuclear test (DPRK2013). Both ^{133}Xe and $^{131\text{m}}\text{Xe}$ were detected in three samples at the IMS station JPX38 and two samples at the IMS station RUX58 after more than 50 days. The activity ratios of

¹ Comprehensive Nuclear-Test-Ban Treaty Organization, Vienna, Austria. E-mail: boxue.liu@ctbto.org

² Lawrence Livermore National Laboratory, Livermore, CA 94550, USA.

³ Stratify LLC/M.H. Chew and Associates, Livermore, CA 94551, USA.

$^{133}\text{Xe}/^{131\text{m}}\text{Xe}$ are consistent with simplified simulations of delayed releases (Ringbom et al., 2014) and with more detailed simulations of radionon accumulated in a void/tunnel due to convection-driven leakage from the explosive cavity/chimney (Carrigan et al., 2016, 2020).

The detonation time of a nuclear explosion can be estimated by using a function of the isotopic activity ratio from the time of detonation up to the time of collection stop based on assumed scenarios, e.g., pairs of ^{140}Ba and ^{140}La , ^{95}Zr and ^{95}Nb , and ^{133}Xe and $^{131\text{m}}\text{Xe}$ (Carrigan et al., 2016; Ringbom et al., 2014; Yamba et al., 2016). If the same decay chain is assumed before a release at the surface and during atmospheric transport, the elapsed time since the time of detonation can be estimated by solving activity evolution equations numerically and/or analytically (Bateman, 1910; Kalinowski et al., 2010; Yamba et al., 2016). The associated uncertainty estimation of the elapsed time can be performed using the Monte Carlo method (MCM) regarding non-linear functions of exponentials and logarithms (ISO/IEC, 2008; Kalinowski & Liu, 2020) and numeric derivatives (ISO, 2019).

Generally, there are three stages of isotopic activity ratios involved from the initial release up to sample measurements. The first one is the ratio of activities of two isotopes at the time of release. The second one is the ratio of activity concentrations in the radioactive air crossing a sampling location at the end of a sample collection period. The third one is the ratio of activities collected in a sample either at the time of collection stop or acquisition start. Some studies used the activity ratio of $^{131\text{m}}\text{Xe}$ to ^{133}Xe determined in the sample measurements for the characterization of the DPRK2013 event, including the estimation of the explosion time (Axelsson & Ringbom, 2014; Ringbom et al., 2014). This differs from investigations using the isotopic ratios of activity concentrations in the plume (Kalinowski, 2011; Kalinowski & Pistner, 2006; Kalinowski et al., 2010). Fundamentally, the isotopic activity ratio, as a function of time (i.e., the curve of activity evolution), needs to be derived for characterizing a nuclear release event. The isotopic ratio of activity concentrations in the plume of air connects the two ends of activity evolution from release to sample

measurement. The activity concentration profile in a plume can be related to the released activities from a UNE by using atmospheric transport modelling (ATM). Since an air mass containing passive tracers (plume) is transported from a nuclear explosion site to a measurement station, ATM simulations provide valuable contributions assuming that the released activities form a linear¹ relationship with activity concentrations in the air mass (Becker et al., 2007; Wotawa et al., 2003).

For isotopic activity ratio analyses based on sample measurements, the first step is to estimate the isotopic ratio of two activity concentrations at the time of collection stop under the assumption of a constant concentration profile during the sampling. The upper and lower limits of the isotopic activity ratio can be estimated using Fieller's theorem (Axelsson & Ringbom, 2014) or Bayesian statistics (Zaehring & Kirchner, 2008) for the event screening flags. Principally, the uncertainty estimation of the explosion time can be based on the propagation of uncertainties (Yamba et al., 2016). However, when the Bateman equations are used for a complicated decay chain, this might turn out to be a non-trivial undertaking and even an impossible one. It is more practical to apply the MCM directly to activities measured in the samples or to associated peak counts in the spectrum analysis, especially in the case of the non-linear relationship between the elapsed time and isotopic activity ratio (Liu & Kalinowski, 2021).

In this paper, the relationships of quantities involved in the three stages of isotopic activity evolution, namely, in the subsurface prior to the release into the atmosphere, in the air mass transported by the wind fields, and in the sample collected at an IMS station, are discussed, including the uncertainty estimation involved. The analysis procedures and results of the IMS observations related to the DPRK2013 nuclear test event, Fukushima Daiichi nuclear disaster and daily radionon background are provided as examples.

¹ This is a simplified source-receptor matrix concept without considering non-linear chemistry.

2. Isotopic Activity Ratio Analysis

2.1. Activities Released from a Nuclear Explosion

The activity evolution from a nuclear explosion up to the release of gases into the atmosphere is a complicated process. It is related not only to radioactive decay chains, but also the convection and diffusion of radioxenon gases from the explosion chimney to the ground surface. The chemistry of precursors to radioxenon isotopes, geology and time of release post-detonation, amongst other factors, can influence the amount of activity released. Radioxenon gases could be accumulating in a tunnel related to the nuclear test, resulting in a delayed release (Carrigan et al., 2016, 2020).

In an ideal and well-mixing system, activities can be estimated based on mass decay/ingrowth chains using Bateman equations (Bateman, 1910; Kalinowski, 2011). The isotopic ratio of released activities is given by:

$$R(t_1) = A_2(t_1)/A_1(t_1). \quad (1)$$

Here, $A_1(t_1)$ and $A_2(t_1)$ are activities of two isotopes (Bq) at time t_1 . The time t_1 marks the start of the release into the atmosphere since the time of detonation.

2.2. Activity Concentrations in the Air over an IMS Station

The radioxenon isotopes that are released from ground or water into the air at t_1 are picked up by the winds and are further subject to the dynamics of the atmosphere. ATM is required to follow the radioxenon isotopes by computing the travel paths from the release location to any other relevant location of reception across the globe. For this, the CTBTO employs the versatile and efficient particle transport model Flexpart (Stohl & Thomson, 1999; Stohl et al., 1998, 2005), which is a Lagrangian particle dispersion model able to perform backward (explicit inverse modelling) and forward tracer transport by computing the so-called source-receptor relationship. This relationship links the relevant start- and end-point of the transport of a unit tracer in an integrated fashion by filling a source-receptor matrix. Source

attribution (e.g., for radioisotopes) can be efficiently done by mere matrix multiplication. The resulting source-receptor sensitivity (SRS) field is expressed as a product of a spatial-temporal source at discrete locations and time intervals through $C_{ijn} = S_{ijn} \times M_{ijn}$, where C is the attributed concentration of the tracer (Bq m⁻³), S is the source attribution (Bq), and M is the source-receptor matrix as a dilution field (m⁻³) (Becker et al., 2007; Kuśmierczyk-Michulec et al., 2021; Stohl et al., 2005; Wotawa et al., 2003).

For our study, we utilize CTBTO's ATM pipeline to produce SRS fields with activity concentrations based on a default nuclear explosion with a strength of 1 Bq (unit source attribution)² (Kuśmierczyk-Michulec et al., 2021). The time resolution is three hours, and the spatial resolution of each SRS matrix element is 0.5 by 0.5 degrees (55 km by 55 km). Obviously, the simulated activity concentration at a measurement site—assuming the plume traverses the site—shows one value every three hours and is constant over a large domain during each timestep compared to an IMS observation, which entails a point location collecting radioxenon isotopes for twelve hours per sample (or sometimes twenty-four hours, depending on the sampling equipment used). Clearly, the space and time parameters differ when comparing or combining activity concentration simulations with observations: [55 km by 55 km every 3 h]_{ATM} vs. [point every 12 h]_{IMS}. We note, however, that the spatial incongruity is not covered in this paper as we focus only on the temporal aspect of matching simulations with observations.

Now we need to match the simulated activity concentrations to the concentration obtained from the measurement at the time of collection stop (after twelve hours of sampling). This can be done by simply computing the average concentration for the four consecutive interval values of three hours. A more accurate approach, however, would consider the short half-lives of certain isotopes for the current

² We could use the dilution matrix directly (to get the m⁻³ quantity), see later in Eq. (2), but activity concentrations based on an initial activity (with default or any strength of choice) are standard output for CTBTO's ATM pipeline studies. Here we choose 1 Bq for convenience.

sampling time, which requires a more comprehensive computation.

When this final simulated activity concentration is computed, it can be divided by the 1 Bq source attribution to get the dilution matrix M in (m^{-3}) at the station. We designate the time of collection stop by t_2 for our backward isotopic analysis and use both $C(t_2)$, the activity concentration measured at the station, and the simulated dilution value in $M(t_2)$ to get $A(t_2)$ through:

$$A(t_2) = \frac{C(t_2)}{M(t_2)}. \quad (2)$$

Using Eq. (2), the isotopic activity ratio at the time of collection stop can be estimated by

$$R(t_2) = \frac{A_2(t_2)}{A_1(t_2)} = \frac{C_2(t_2)/M(t_2)}{C_1(t_2)/M(t_2)} = \frac{C_2(t_2)}{C_1(t_2)}. \quad (3)$$

Regarding the activity evolution, the isotopic ratio in Eq. (3) is defined by the released activities of the source term first but estimated by activity concentrations in the air mass passing the sampling location in the end.

The isotopic activity ratio at the release site using Eq. (1) needs to be related to the ratio at the IMS station in Eq. (3), through the ATM assumption in Eq. (2). Since for ATM part a universal tracer is applied (though source attributed), the activity decay during forward transport is not included in Eq. (2) but can be processed a posteriori to get a decay corrected dilution value (for each radionuclide of relevance). The impact on the isotopic ratio estimation caused by the concentration profile and decay correction during sampling are being investigated and will be presented in the future.

2.3. Activities Collected in Samples at the IMS station

Activity concentrations are assumed to be constant during sampling. Therefore, the activities collected in a sample at the time of collection stop are estimated by Eq. (4), irrespective of an independent decay or parent-daughter decay chain.

$$A_s(t_2) = C(t_2)V_s \frac{1 - e^{-\lambda t_c}}{\lambda \tau_c}, \quad (4)$$

where, V_s is the air volume sampled (m^3), the subscript s indicates the activity collected in the sample; λ is the decay constant (s^{-1}); τ_c is the duration of collection (s); $A_s(t_2)$ is the activity collected in the sample at the time of collection stop. The activity concentration is referenced at the time of collection stop in Eq. (4), which is consistent with Eq. (3).

Using Eq. (3) and (4), the isotopic ratio of activity concentrations in the plume of air is related to the isotopic ratio of activities collected in the sample at the collection stop time, $R_s(t_2)$, by:

$$R_s(t_2) = \frac{A_{2s}(t_2)}{A_{1s}(t_2)} = R(t_2) \frac{\lambda_1}{\lambda_2} \frac{1 - e^{-\lambda_2 \tau_c}}{1 - e^{-\lambda_1 \tau_c}}. \quad (5)$$

The isotopic ratio of activities collected in the sample is dependent on the decay constants (λ_1 , λ_2) as well as the collection time τ_c . In contrast, the isotopic ratio of activity concentration in the plume of air in Eq. (3) is only dependent on decay parameters. Therefore, the isotopic ratio of activity concentrations in the plume instead of the isotopic ratio of activities collected in the sample is used to characterize the activity evolution from the time of detonation until sample measurement, as indicated in Eqs. (1) and (3).

2.4. Activities Measured at the Time of Acquisition Start

For an independent decay, the activity $A_{1s}(t_3)$ (Bq) collected in the sample at the time of acquisition start (t_3) is determined by Eq. (6).

$$A_{1s}(t_3) = \frac{x_1}{\varepsilon_1 BR_1} \frac{\lambda_1}{1 - e^{-\lambda_1 \tau_a}} \quad (6)$$

where x_1 is the net number of counts for an isotope 1 (the subscript indicates an independent isotope or the parent isotope of a parent-daughter decay chain) determined in spectrum analysis; ε_1 is the efficiency; BR_1 is the branching ratio; τ_a is the real acquisition time (s) of the spectrum.

For a decay chain of parent to daughter, the activity of the daughter isotope is estimated by Eq. (7).

$$A_{2s}(t_3) = \frac{x_2}{\varepsilon_2 BR_2} \frac{\lambda_2}{1 - e^{-\lambda_2 \tau_a}} - A_{1s}(t_3) \frac{\lambda_2}{\lambda_2 - \lambda_1} \left(\frac{\lambda_2}{\lambda_1} \frac{1 - e^{-\lambda_1 \tau_a}}{1 - e^{-\lambda_2 \tau_a}} - 1 \right). \quad (7)$$

After the collection stop, there is a processing period (τ_p), the decay time of 24 h for particulate samples or the processing time of a few hours for noble gas samples. Considering decay corrections, the activity for the parent isotope, $A_{1s}(t_2)$, and the activity for the daughter isotope of parent-daughter decay chain, $A_{2s}(t_2)$, at the time of collection stop can be estimated by Eqs. (8) and (9), respectively.

$$A_{1s}(t_2) = A_{1s}(t_3) e^{\lambda_1 \tau_p} \quad (8)$$

$$A_{2s}(t_2) = \left(A_{2s}(t_3) - A_{1s}(t_3) \frac{\lambda_2}{\lambda_2 - \lambda_1} \left(1 - e^{-(\lambda_2 - \lambda_1) \tau_p} \right) \right) e^{\lambda_2 \tau_p}. \quad (9)$$

Sampling is completed at the collection stop time. Activities collected in the sample depend on decay chains and further processing of samples. The collected sample might be measured by using different approaches, such as re-analysis in IMS radionuclide laboratories. It would be very practical to give the activities referenced at the time of collection stop, especially for the estimation of activity concentrations.

Applying Eqs. (8) and (9) into Eq. (5), the isotopic ratio of activity concentrations at the time of collection stop, $R(t_2)$, based on the sample measurement, is estimated by Eq. (10).

$$R(t_2) = \frac{\lambda_2}{\lambda_1} \frac{1 - e^{-\lambda_1 \tau_c} e^{-\lambda_1 \tau_p}}{1 - e^{-\lambda_2 \tau_c} e^{-\lambda_2 \tau_p}} \left[\frac{A_{2sT}(t_3)}{A_{1s}(t_3)} - \frac{\lambda_2}{\lambda_2 - \lambda_1} \left(\frac{\lambda_2}{\lambda_1} \frac{1 - e^{-\lambda_1 \tau_a}}{1 - e^{-\lambda_2 \tau_a}} - e^{-(\lambda_2 - \lambda_1) \tau_p} \right) \right] \quad (10)$$

where $A_{2sT}(t_3) = \frac{x_2}{\varepsilon_2 BR_2} \frac{\lambda_2}{1 - e^{-\lambda_2 \tau_a}}$ indicates the activity of the daughter isotope determined by the peak counts without the parent-daughter decay correction (subscript T), which is the same as Eq. (6).

Applying Eqs. (6) and (7) into Eq. (10), the isotopic ratio of activity concentrations at the time of collection stop is estimated by Eq. (11), based on net numbers of peak counts.

$$R(t_2) = \frac{\lambda_2}{\lambda_1} \frac{1 - e^{-\lambda_1 \tau_c} e^{-\lambda_1 \tau_p}}{1 - e^{-\lambda_2 \tau_c} e^{-\lambda_2 \tau_p}} \left[\frac{x_2}{x_1} \frac{\varepsilon_1 BR_1}{\varepsilon_2 BR_2} \frac{\lambda_2}{\lambda_1} \frac{1 - e^{-\lambda_1 \tau_a}}{1 - e^{-\lambda_2 \tau_a}} - \frac{\lambda_2}{\lambda_2 - \lambda_1} \left(\frac{\lambda_2}{\lambda_1} \frac{1 - e^{-\lambda_1 \tau_a}}{1 - e^{-\lambda_2 \tau_a}} - e^{-(\lambda_2 - \lambda_1) \tau_p} \right) \right]. \quad (11)$$

2.5. Analysis Procedure

Activities released from a nuclear event, activity concentrations in the plume passing over an IMS station, and activities collected in a sample at the IMS station can be related based on an analysis procedure including the activity evolution from an assumed UNE, through ATM simulations, to sample measurements. The activity concentrations in the plume serve a key role between release and sample measurement. On the one hand, activities released from a nuclear explosion can be estimated based on an assumed scenario in order to have the predicted activity concentrations at a station based on the forward ATM simulations. On the other hand, activities collected in the sample are determined based on spectra analysis and the accompanying activity concentrations are estimated under the assumption of the concentration profile during sampling. As mentioned above, the isotopic ratio of activities collected in the sample differs from the one of activity concentrations in the plume as shown in Eqs. (1), (3), and (5). It is a backward procedure to estimate the isotopic ratios of activity concentrations in the plume, based on activities measured in the sample, as shown in Fig. 1.

3. Source Term of a Nuclear Explosion

3.1. Schematic Sequence of an Underground Nuclear Explosion

The sequence of cavity evolution following a UNE is illustrated by (Carrigan et al., 2020). During

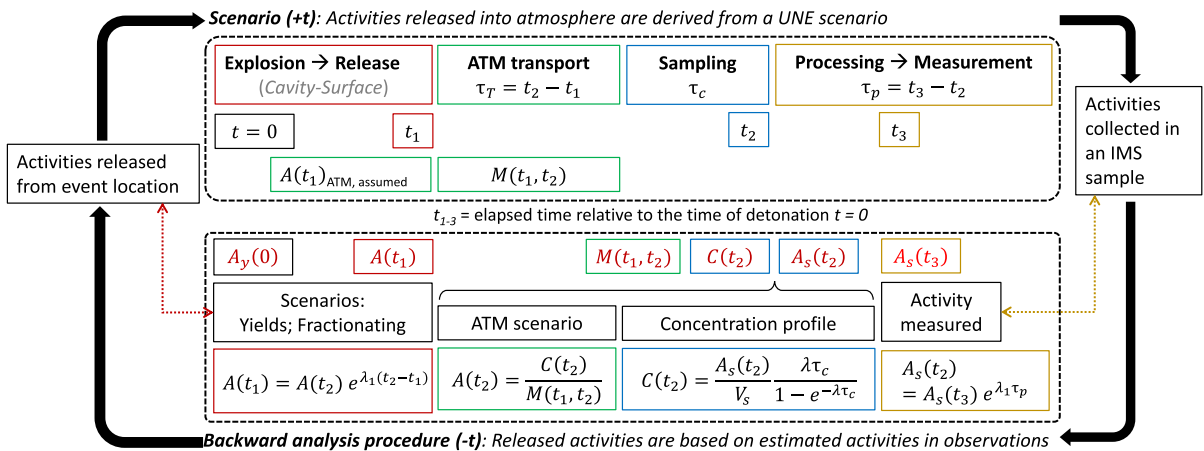


Figure 1

Schematic sequence of processes from the explosion ($t = 0$) to the release time (t_1), the collection stop time (t_2), and the acquisition start time (t_3). In contrast, the analysis is performed in reverse order, from the activity measured in the sample back to the activity released. See the text for descriptions of all the quantities and formula

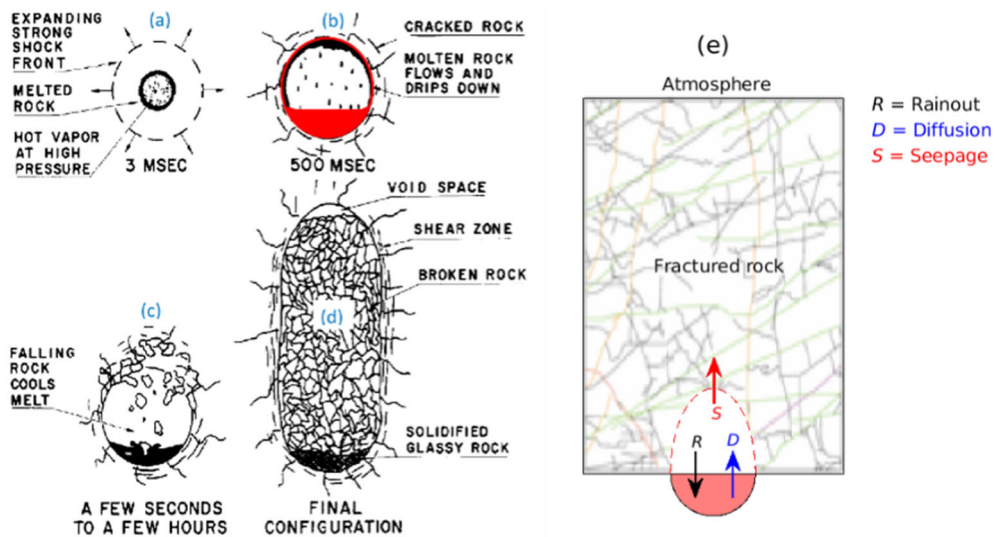


Figure 2

The sequence of events giving rise to the zone of melt at the bottom of a UNE cavity and chimney is illustrated by (Schwartz et al., 1984) as periods of **a** cavity expansion, **b** rock melting, **c** cavity collapse, and **d** chimney formation. The conceptual model of source-term activities is referred to Sun et al. (2021). R , D , and S in the cavity represent rainout, back diffusion, and seepage, respectively, in **e**

the rapid expansion of a detonation cavity following a UNE (Fig. 2a), high pressure and temperature result in the formation of a melt zone on the walls of the cavity and form a melt puddle at the bottom of the cavity resulting in a two-phase system with a volatile gas and vapor overlying a zone of melted rock

(Fig. 2b). During the rapid cooling of the vapor phase, the vaporized iodine precursors condense out, mixing with the melt phase in the puddle, while some small fraction of the radioxenon isotopes produced in the puddle may possibly be transported back to the gas phase in the cavity. Collapse of the cavity/

chimney may enhance gas seepage and/or prompt venting of radioxenon isotopes produced from decay/ingrowth in the cavity (Fig. 2c, d).

3.2. Bateman Equation

Released activities can be estimated based on mass decay chains using the Bateman equation Eq. (12) (Bateman, 1910; Kalinowski, 2011; Kalinowski & Pistner, 2006).

$$N_{m,n}(t) = \sum_{k=1}^n \left[N_{m,k}^0 \cdot \prod_{l=k}^{n-1} b_{m,l} \cdot \sum_{j=1}^n \left(\frac{\tau_{m,n}}{\tau_{m,j}} \cdot \prod_{i=1}^{n-1} \frac{1}{1 - \frac{\tau_{m,i}}{\tau_{m,j}}} e^{-\ln 2 \cdot t / \tau_{m,j}} \right) \right] \quad (12)$$

where, t is the elapsed time relative to the time of detonation; $N_{m,n}(t)$ is the number of the n -th nuclide in the mass chain m at the time t ; $\tau_{m,n}$ is the half-life of the n -th nuclide in the mass chain m . Independent fission yields $N_{m,k}^0$ and decay branching fractions $b_{m,l}$ are taken from (England & Rider, 1994). The Bateman equation for a given mass chain is solved numerically for each time frame. All possible paths through the branches of the decay chain are treated individually and the results are added up.

Due to the isotope separation from their precursors, the parameters related to decay chains need to be adjusted accordingly, such as assumed modes of full- and part-ingrowth. For example, radioxenon decay chains are evolving along with their iodine precursors in the chimney after a UNE. However, after release at the surface, iodine isotopes might be separated completely and only the radioxenon isotopes are transported in the plume.

3.3. Analytical Solution Development

Carrigan et al. (2020) and Sun et al. (2021) described source-term activities (rainout from cavity to puddle, back diffusion from puddle to cavity, and seepage from the cavity to host rock, see Fig. 2e) together with radioactive decay/ingrowth using ordinary differential equations (ODEs)

$$\frac{d\mathbf{c}}{dt} = \mathbf{A}\mathbf{c} = (\mathbf{S}\mathbf{A}\mathbf{S}^{-1})\mathbf{c}. \quad (13)$$

In Eq. (13), \mathbf{c} is the vector of concentrations, t is time, \mathbf{A} is the reaction matrix describing radioactive decay/ingrowth and source-term activities, \mathbf{S} is the matrix whose columns are the eigenvectors of \mathbf{A} , \mathbf{S}^{-1} is the inverse matrix of \mathbf{S} and $\mathbf{\Lambda}$ is the eigenvalue matrix of \mathbf{A} .

Defining $\mathbf{a} = \mathbf{S}^{-1}\mathbf{c}$,

$$\frac{d\mathbf{a}}{dt} = \mathbf{\Lambda}\mathbf{a} \quad (14)$$

is solved analytically. The solution of \mathbf{c} is derived using “ $\mathbf{c} = \mathbf{S}\mathbf{a}$ ” as

$$\mathbf{c}(t) = \mathbf{S} \begin{bmatrix} \exp(\lambda_n t) & \cdots & 0 \\ \vdots & \ddots & \vdots \\ 0 & \cdots & \exp(\lambda_n t) \end{bmatrix} \mathbf{S}^{-1}\mathbf{c}_0 \quad (15)$$

where, \mathbf{c}_0 is the vector of initial concentrations. For details of the analytical formulation of \mathbf{S} and \mathbf{S}^{-1} , the reader is referred to Sun et al. (2015) and Sloan et al. (2016).

3.4. Verification and Inter-Code Comparison

Because of the stiffness of ODEs involving a large difference (e.g., 6-orders of magnitude) in half-lives, an additional effort is required to obtain convergent solutions numerically. Although advanced ODE solvers are available (e.g., ode23s in MATLAB) for dealing with possible stiff reactions, closed-form solutions are preferred due to the extra computational expense of numerical solutions. In addition, closed-form solutions are required for the verification of numerical codes, which can be utilized in solving more complex and practical problems. For comparison purposes, we simulated radioxenon mass using both closed-form solution and solving ODEs using ode23s (MathWorks, 2000) and compared solutions in Fig. 3.

We simulated radioxenon production and decay from decay chains 131, 133, and 135 in a closed system using the independent yields and half-lives provided by England and Rider (1994). For this

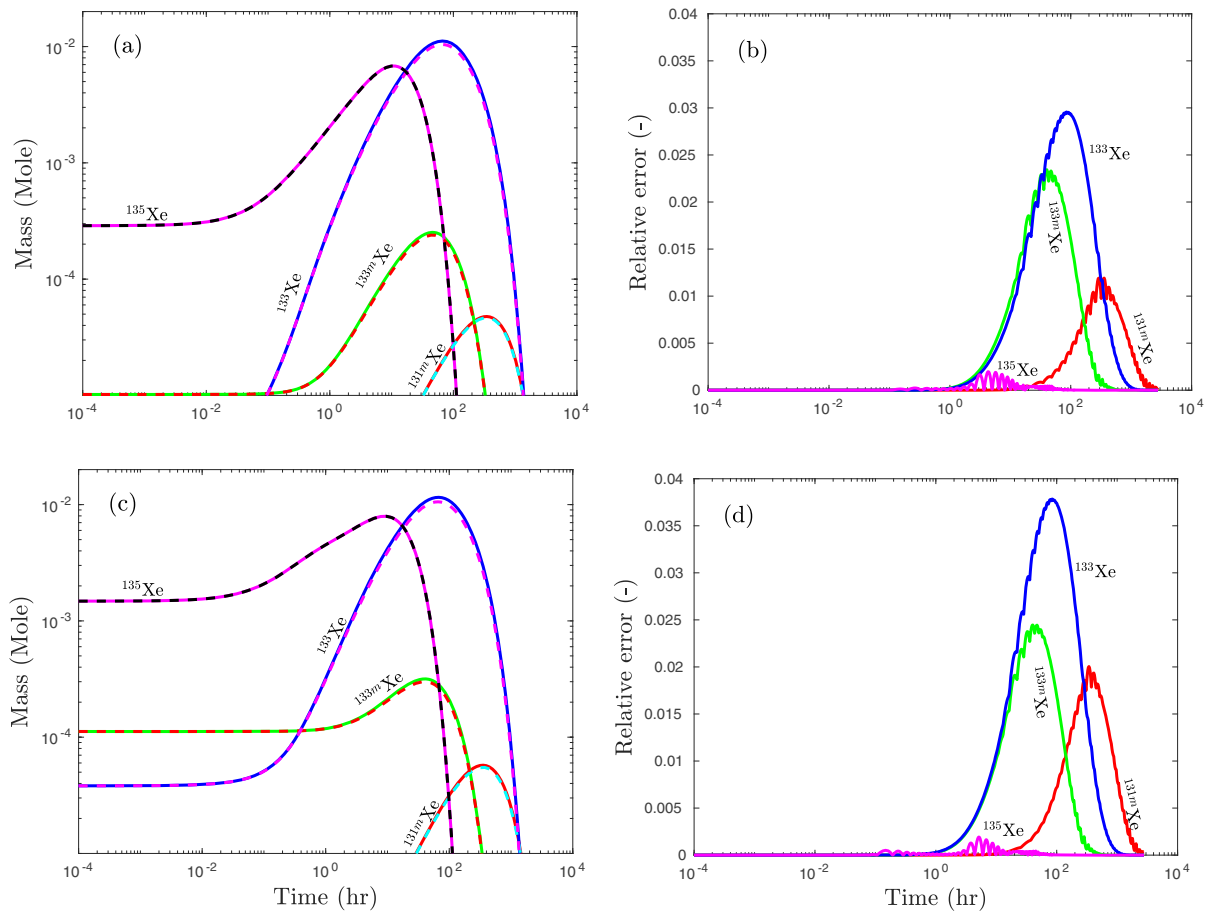


Figure 3

Comparison of analytical and numerical solutions of radioxenon inventories in a closed cavity. **a** Radioxenon inventories from $1\text{kt } ^{235}\text{fU}$. **b** Relative error between analytical and numerical solutions for $1\text{kt } ^{235}\text{fU}$. **c** Radioxenon inventories from $1\text{kt } ^{239}\text{fPu}$. **d** Relative error between analytical and numerical solutions for $1\text{kt } ^{239}\text{fPu}$. Solid and dashed lines in **a** and **c** represent analytical and numerical solutions, respectively

benchmark problem, a few computer codes are available. Among those codes, ORIGEN is the most accepted computer code for calculating the buildup, decay, and processing of radioactive materials. ORIGEN uses a matrix exponential method to solve a large system of coupled, linear, first-order ODEs with constant coefficients. The main disadvantage of the regular Taylor expansion used in ORIGEN is that it is subject to roundoff error especially for stiff systems. Similarly, numerical ODE solvers, such as MATLAB ode23s using a low-order method, are often used for simulating radionuclide decay and ingrowth. For comparison purposes, MATLAB ode23s is used by LLNL to obtain a numerical solution. However, numerical solutions are subject to

high computational expense and convergence issues. For this reason, analytical (closed-form) solutions are preferred. The IDC (International Data Center) solution (Kalinowski, 2011; Kalinowski & Pistner, 2006) and Yamba's model (Yamba et al., 2016) are purely analytical solutions modified from the Bateman equation and implemented differently in a MATLAB environment. The LLNL analytical model (Sloan et al., 2016; Sun et al., 2015) is a flexible solution using analytical singular-value decomposition. It is purely functional and flexible to user-defined decay-ingrowth structure. It is noted that the decay-ingrowth of decay chains 131, 133, and 135 is a stiff problem with minimum and maximum half-lives of 0.18 (s) and 11.84 (d). The time scale is 5.6832×10^6

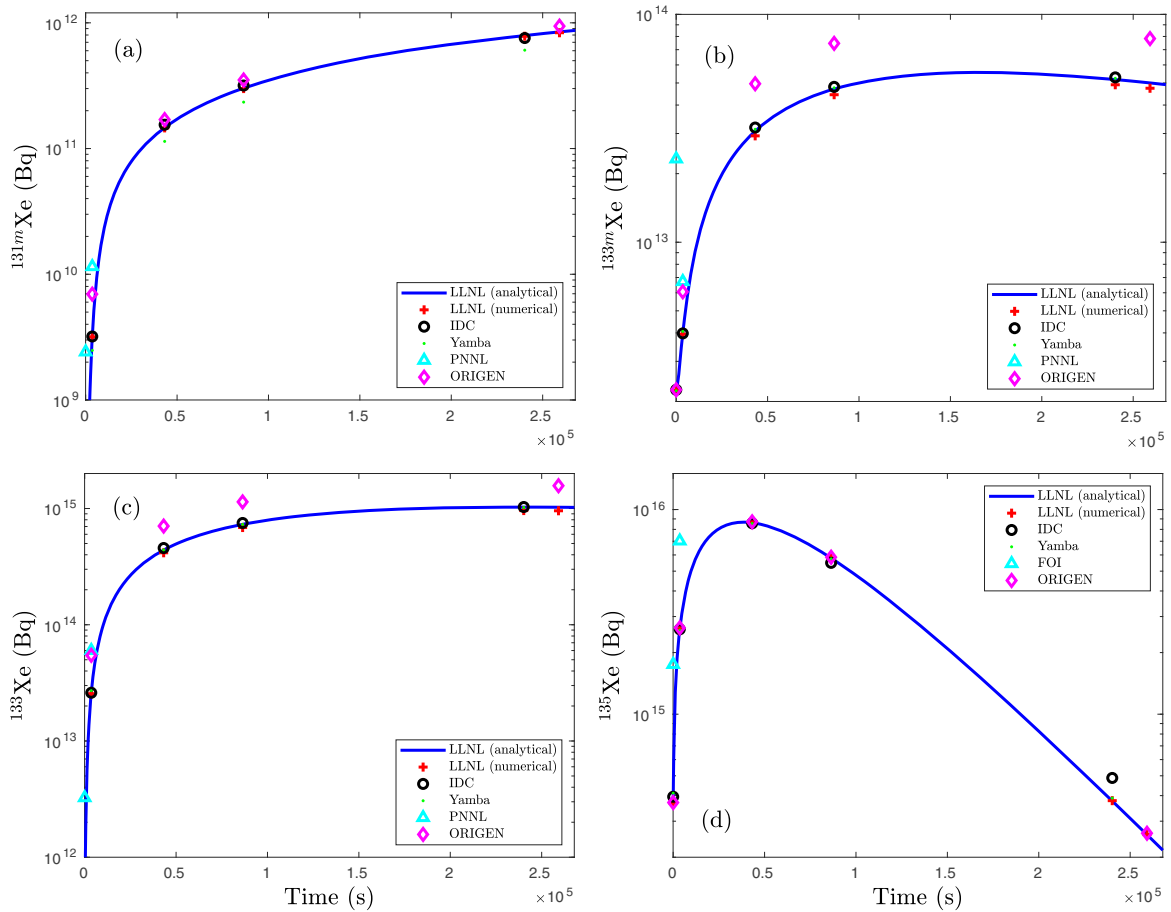


Figure 4
Inter-code comparison of radioxenon ratio of activities (a) ^{131m}Xe , b) ^{133m}Xe , c) ^{133}Xe , and d) ^{135}Xe for 1kt ^{235}fU

times different and independent yields are also orders of magnitude different. For this reason, the inter-code comparison is plotted on log10 scale in Figs. 4 and 5 for ^{235}fU and ^{239}fPu , respectively.

3.5. Impact of Source-Term Activities on Relationship of Four Radioxenon Isotopes

Figure 6 shows the fully fractionated (instantaneously produced or independent yield) and unfractionated (solid blue curve) evolutionary correlations of $^{133m}\text{Xe}/^{131m}\text{Xe}$ and $^{135}\text{Xe}/^{133}\text{Xe}$. Assuming rainout rates of iodine precursors, back diffusion rate, and seepage rate, Sun et al. (2021) compared the four radioxenon plot with and without source-term

activities in Fig. 6. The four radioxenon plot depends on sample locations and source-term activities.

4. Calculation of Isotopic Activity Ratios

The concentration and associated uncertainty values are given in IDC analysis reports. The nominal value r_0 and the associated uncertainty $u(r_0)$ of the isotopic activity ratio are estimated by Eq. (16),

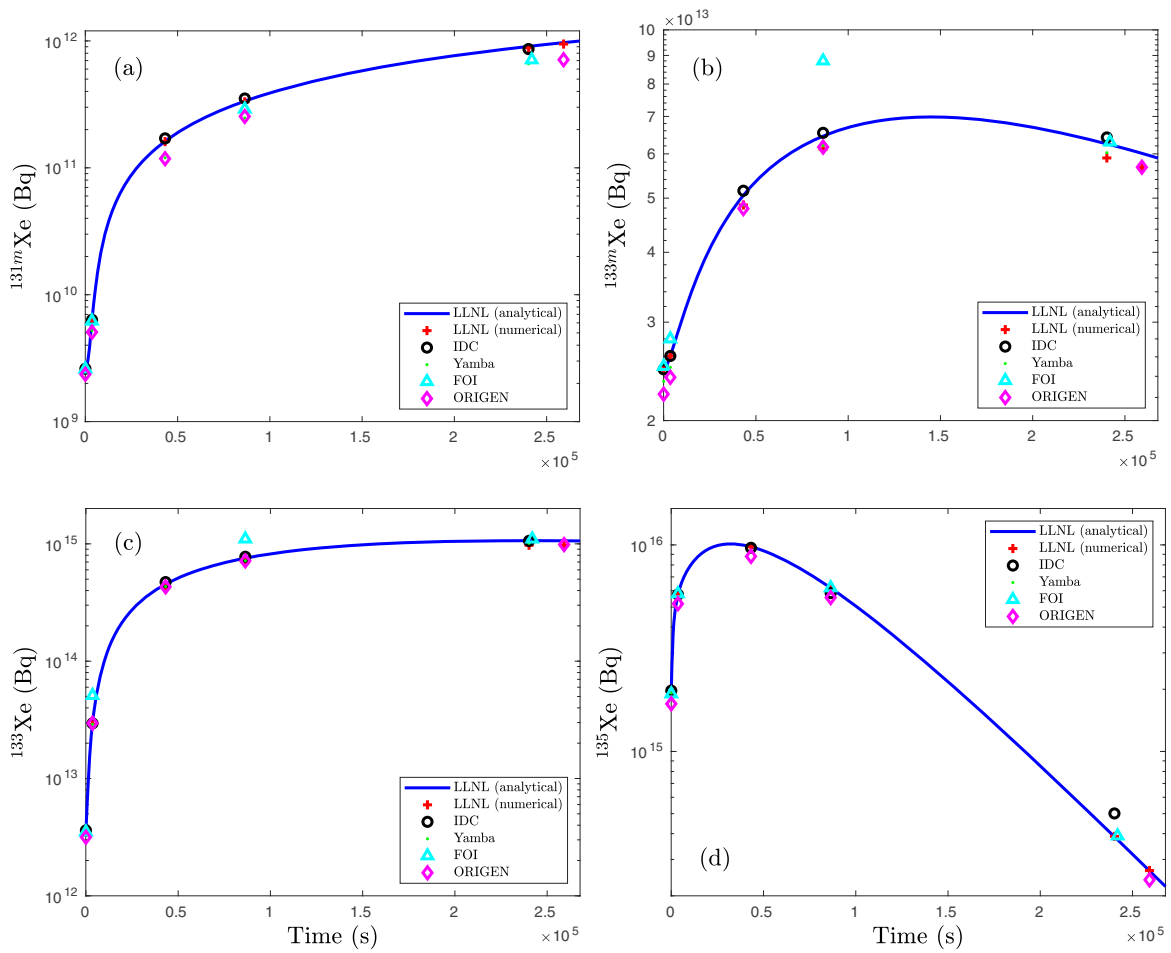


Figure 5
Inter-code comparison of radioxenon ratio of activities (a ^{131m}Xe , b ^{133m}Xe , c ^{133}Xe , and d ^{135}Xe) for 1kt ^{239}fPu

$$r_0 = \frac{c_2}{c_1},$$

$$u^2(r_0) = r_0^2 \left(\frac{u^2(c_1)}{c_1^2} + \frac{u^2(c_2)}{c_2^2} - 2 \frac{\text{Cov}(c_1, c_2)}{c_1 c_2} \right). \quad (16)$$

Notice that r_0 in Eq. (16) is calculated from the values of activity concentrations, c_1 and c_2 , as taken from analysis reports. However, $R(t_2)$ in Eq. (3) is defined as the ratio of two random variables, i.e., the activity concentrations $C_1(t_2)$ and $C_2(t_2)$. There is no formula for calculating the expectation and variance of a ratio of random variables without reference to any specific probability distribution. The way forward is to perform a Taylor expansion of $E[R(C_1, C_2)]$ and $\text{Var}[R(C_1, C_2)]$ at the values c_1 and

c_2 , the results of which in first order are then the values of Eq. (16). By extending the Taylor expansion to the second order, we obtain the ratio r and the associated uncertainty $u(r)$, as shown in Eq. (17).

$$r = r_0 \left(1 + \frac{u^2(c_1)}{c_1^2} - \frac{\text{Cov}(c_1, c_2)}{c_1 c_2} \right), u^2(r) = r_0^2 \left(\frac{u^2(c_2)}{c_2^2} \left(1 + 3 \frac{u^2(c_1)}{c_1^2} \right) + \frac{u^2(c_1)}{c_1^2} \left(1 + 8 \frac{u^2(c_1)}{c_1^2} \right) - 2 \frac{\text{Cov}(c_1, c_2)}{c_1 c_2} \right). \quad (17)$$

The biases are mainly dependent on the uncertainty of the denominator, as shown in Eq. (17),

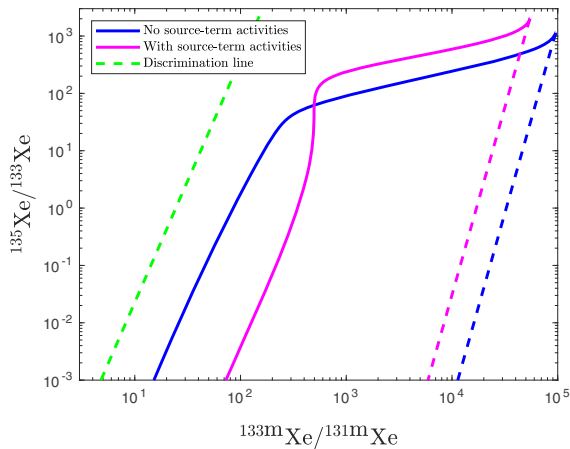


Figure 6

Four radioxenon plot in the cavity with and without source-term activities (re-plotted from Sun et al., 2021, Fig. 8a). The green dashed line is the discrimination between civilian applications (left) and UNEs (right). Other two dashed lines indicate the evolution of the activity ratios of xenon isotopes created at detonation only

especially with large relative uncertainties of the concentrations for low-level samples.

Differing from the analytical approach described above, a numerical approach utilizing the MCM can accomplish the propagation of probability distributions (ISO/IEC, 2008). The analysis model is dependent on the measurement process and the spectrum analysis of the sample. First, the values of input parameters, such as activity concentrations from the analysis report or original peak counts from the spectrum, are sampled based on associated probability distributions. Then the distributions of isotopic activity ratios and/or explosion times are derived. Finally, the mean values of isotopic activity ratios and/or detonation times, associated uncertainties and limits of the coverage interval are estimated accordingly (Liu & Kalinowski, 2021).

5. Results and Discussion

5.1. Observations at IMS Stations

After more than 50 days following the announced third DPRK nuclear test event in 2013, three consecutive Level C samples at JPX38 and two consecutive Level C samples at RUX58 were considered that might have originated from this event

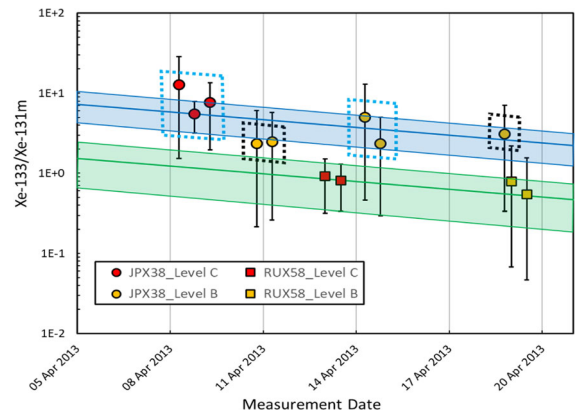


Figure 7

Decay consistent analysis of isotopic activity ratios for three Level C samples at JPX38, two Level C samples at RUX58 as well as the Level B samples in the period. Level B samples marked by a blue dotted box are associated with the level C samples at JPX38, confirmed by the so-called possible source region analysis resulting from ATM simulations (Kijima et al., 2022). The ratio values are given with second order polynomial and the error bars are the limits of the coverage interval with 95%

(Carrigan et al., 2016, 2020; Ringbom et al., 2014). These five samples as well as the samples related to the Fukushima nuclear disaster and daily radioxenon background at IMS stations are provided as examples demonstrating the described procedures of the isotopic activity ratio analysis.

5.2. Sample Association with the Same Event

The consistency of activity ratios across multiple isotope observations with respect to a given radioactive decay curve is a plausible indication that these isotopes have originated from the same source. For three level C samples (red dot) from JPX38 in Fig. 7, the blue decay curve was estimated using the second sample due to smaller relative uncertainties of concentrations, including the blue bandwidth (the upper and lower limits of the coverage interval under the probability of 95%). For two samples from RUX58 (red squares), the second sample was used to derive the green decay curve and its bandwidth. The isotopic activity ratios of three Level C samples at JPX38 are consistent with a blue decay curve within the blue bandwidth, and two Level C samples at RUX58 with the green decay curve and its bandwidth. The blue bandwidth does not overlap with the

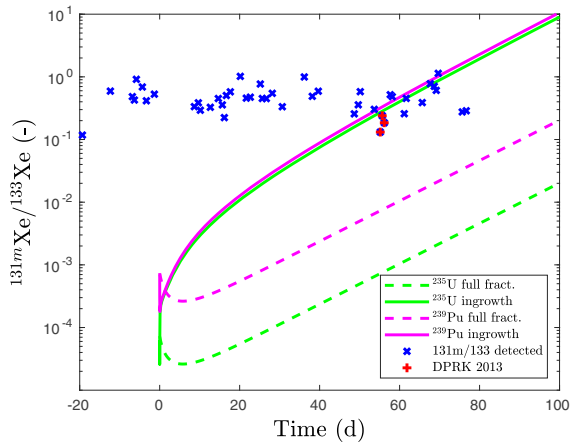


Figure 8

Isotopic activity ratios of $^{131\text{m}}\text{Xe}$ to ^{133}Xe in daily samples at JPX38. The values of isotopic activity ratios related to DPRK2013 are in the range of daily samples during the selected period (the day zero is the date of the announced DPRK2013 event). Ratio values are presented with the nominal values, but their associated uncertainties are not given, which are in the range of (16%, 140%) with the median of 59% in one standard uncertainty

green bandwidth. This indicates that there were two distinct releases at the DPRK test site from the viewpoint of decay-consistent isotopic activity ratios.

Moreover, ATM simulations might improve confidence in sample association by identifying the air masses that link a release to multiple samples. It might be possible that the Level B samples that overlap with the blue bandwidth can be associated with these three Level C samples at JPX38. For this confirmation, a so-called possible source region (PSR) analysis is performed based on correlation algorithms used on SRS fields and radionuclide observations. The results of PSR analysis, see Fig. 8 in (Kijima et al., 2022), indicate that the level B samples marked by a blue dotted box in Fig. 7 are associated with the three level C samples at JPX38. So, it might be possible that these samples originate from the same release. On the other hand, the Level B samples marked by black dotted boxes in Fig. 7 are not associated with these Level C samples indicating they have not originated from the same release.

The criteria for associating relevant episode samples using consistent isotopic activity ratios as well as the analysis procedure combined with ATM simulations are investigated in an ongoing study.

5.3. Combined Analysis Between Activity Concentrations and Isotopic Activity Ratios

The activity ratios of $^{131\text{m}}\text{Xe}/^{133}\text{Xe}$ of the three level C samples at JPX38 related to the DPRK2013 event shown in Fig. 8 are between 0.1 and 1. This is within the range of daily values at JPX38 during the selected period. Whereas Fig. 9 shows an example of the activity ratios of $^{131\text{m}}\text{Xe}/^{133}\text{Xe}$ are increasing with time because they are related to the release sources from the Fukushima nuclear disaster. There were several releases. The main reason for the linear shape of the entries is the dilution and the decay over time when the plume traveled through the atmosphere. The ratios related to earlier releases in Fig. 9 are also in the range between 0.1 and 1 in Fig. 8. Considering the activity concentration values instead of the isotopic activity ratios, the daily samples are clearly separated from the Fukushima nuclear disaster and the DPRK2013 samples, as demonstrated in Fig. 10. The activity concentrations of both $^{131\text{m}}\text{Xe}$ and ^{133}Xe in the three level C samples associated with DPRK2013 (red triangles) lie outside of the domain of the general radioxenon background at JPX38 (blue dots) as well as below the ones from the Fukushima nuclear accident (purple diamond). Therefore, both values of isotopic activity ratios and associated activity concentrations need to be scrutinized with respect to assumed scenarios and related ATM simulations.

5.4. Estimation of the Elapsed Time since the Time of Detonation

In one case study, the isotopic activity ratio and elapsed time for one of the samples related to the DPRK2013 nuclear test event were estimated using the MCM. For the sample at JPX38 at 19:00 on 8 April 2013 (collection stop), the concentrations are ^{133}Xe 3.05 ± 0.14 (one standard deviation unless otherwise stated) and $^{131\text{m}}\text{Xe}$ 0.57 ± 0.11 (mBq m^{-3}). For the isotopic ratio of ^{133}Xe to $^{131\text{m}}\text{Xe}$ in Eqs. (16) and (17), the nominal and second order polynomial values are 5.35 ± 1.06 and 5.55 ± 1.20 , respectively. The bias is due to the relative uncertainty of 19% for $^{131\text{m}}\text{Xe}$ in the denominator.

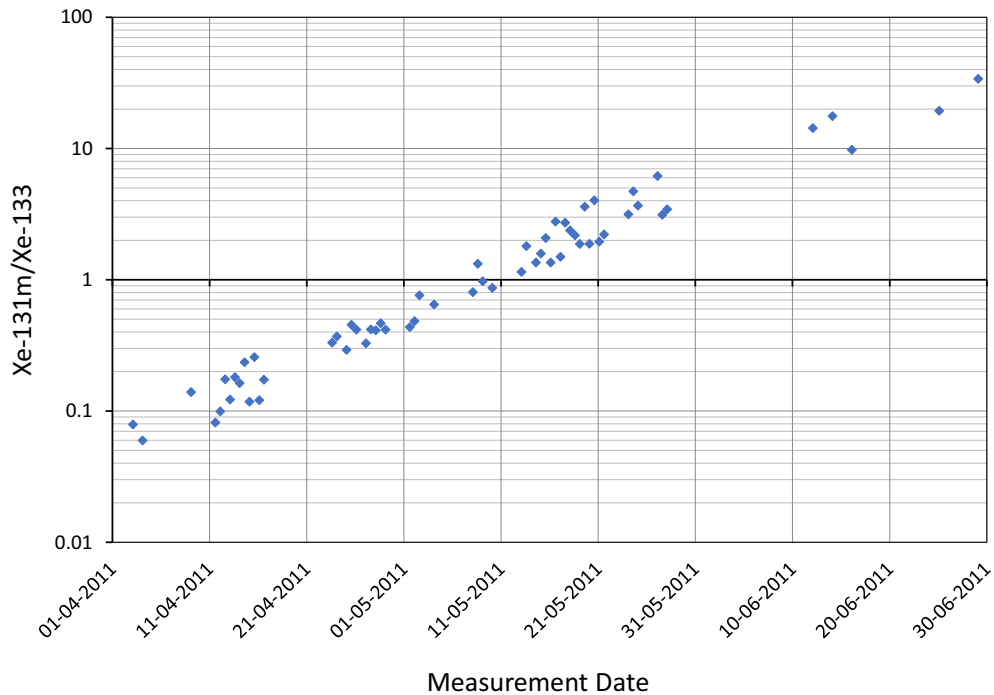


Figure 9

Isotopic activity ratios of $^{131\text{m}}\text{Xe}$ to ^{133}Xe in samples at JPX38 from 1 April to 30 June 2011 are increasing with time due to the release sources from the Fukushima nuclear disaster. Ratio values are presented with the nominal values, but their associated uncertainties are not given, which are in the range of (5%, 39%) with the median of 15% in one standard uncertainty

The isotopic ratios in the activity concentration model in Eq. (3) were estimated by the MCM, where Gaussian distributions for two activity concentrations were used. Both distributions of isotopic activity ratios and elapsed times were estimated accordingly, which differ slightly from the fitted Gaussian curves in Fig. 11a, b. This is due to the exponentials and logarithms involved as well as the relative uncertainty of 19% for $^{131\text{m}}\text{Xe}$. The isotopic ratio of activity concentrations of $^{133}\text{Xe}/^{131\text{m}}\text{Xe}$ is 5.59 ± 1.29 , different from the nominal value of 5.35 ± 1.06 but within one standard uncertainty. Under a simplified full-ingrowth model, the mean values of elapsed times since the time of detonation are 47.3 ± 2.5 and 45.5 ± 2.4 days for the fission material ^{235}U and ^{239}Pu respectively, which are close to the actual 54.5 days. The parameters and assumptions involved need to be further investigated, such as the model based on activities or net numbers of peak counts, or even directly based on the gross numbers of peak counts in the net count calculation method

used for the beta-gamma coincidence spectrum analysis.

5.5. Four Radioxenon Plot

In the case of the DPRK2013 event, only radioxenon isotopes ^{133}Xe and $^{131\text{m}}\text{Xe}$ were detected, therefore, the four radioxenon plot was not applicable. In the case of Fukushima nuclear accident in 2011, all four radioxenon isotopes were detected in a few samples at JPX38. Due to the scale of this incident, anomalous radioxenon detections were frequently observed. As shown in Fig. 12, the detections from the Fukushima nuclear disaster are in the domain of nuclear facility releases, inside the evolution trajectory of the isotopic activity ratios through three reactor circles of LWR burn-up for 3.2% ^{235}fU enrichment.

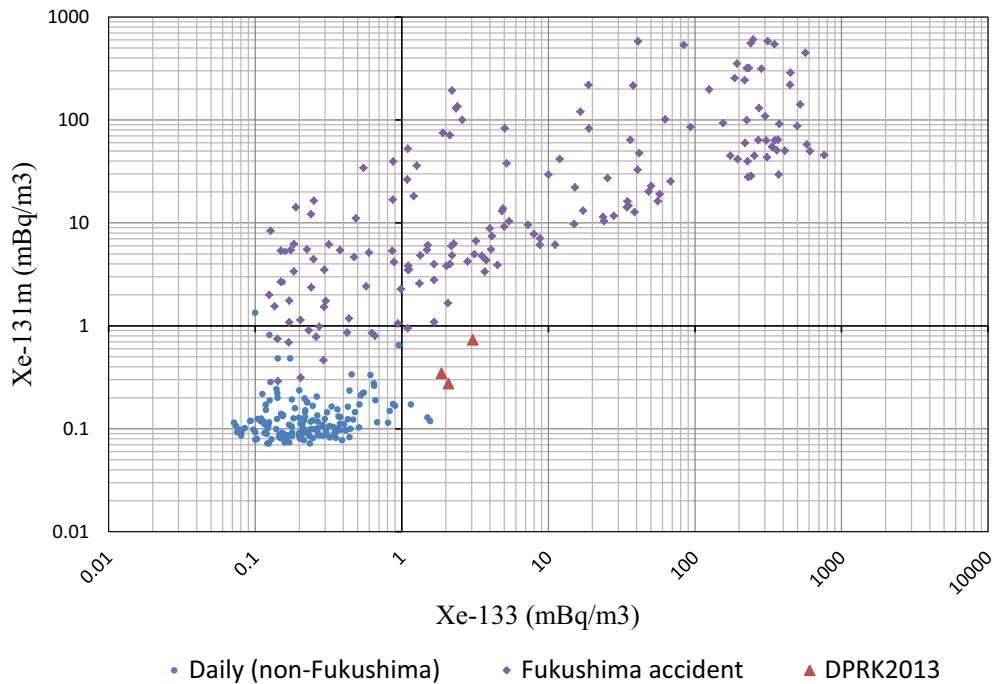


Figure 10

Scatter plot for a pair of activity concentrations, ^{133}Xe versus $^{131\text{m}}\text{Xe}$. The daily samples from 1 July 2011 to 30 April 2013 are clearly separated from the Fukushima nuclear disaster and DPRK2013 samples. Uncertainties of activity concentrations are not presented

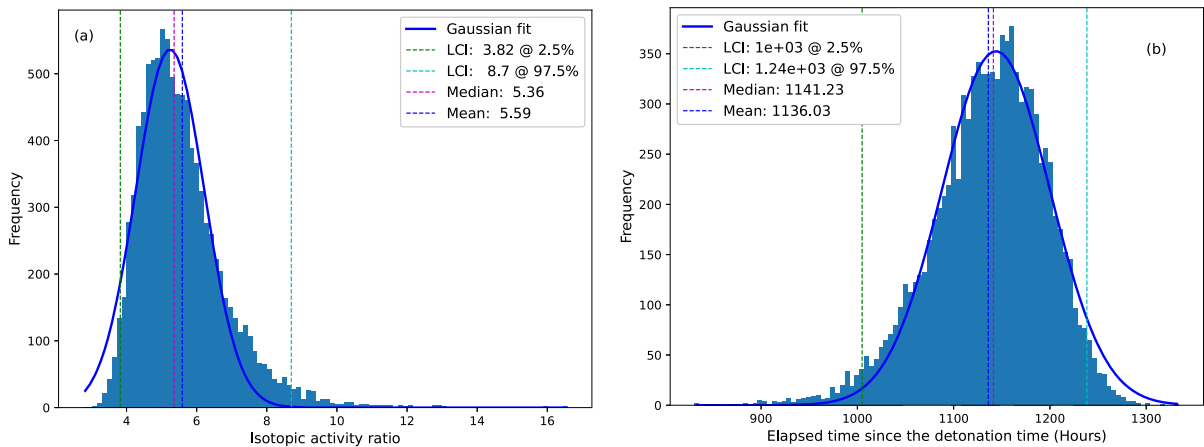


Figure 11

Distributions of isotopic activity ratios and elapsed times derived by MCM under the assumption of a simplified full-ingrowth model for ^{235}U for the DPRK2013 sample at JPX38 at 19:00 on 8 April 2013 (collection stop). Gaussian distribution of inputs concentrations of ^{133}Xe : 3.05 ± 0.14 and $^{131\text{m}}\text{Xe}$: 0.57 ± 0.11 (mBq m^{-3}). **a** Distribution of isotopic activity ratios $^{133}\text{Xe}/^{131\text{m}}\text{Xe}$; **b** Distribution of elapsed times (hours). The mean value of elapsed times is 47.3 days with the limits of the coverage interval for 95% (41.7, 51.7) days compared with the nominal value of 47.6 days

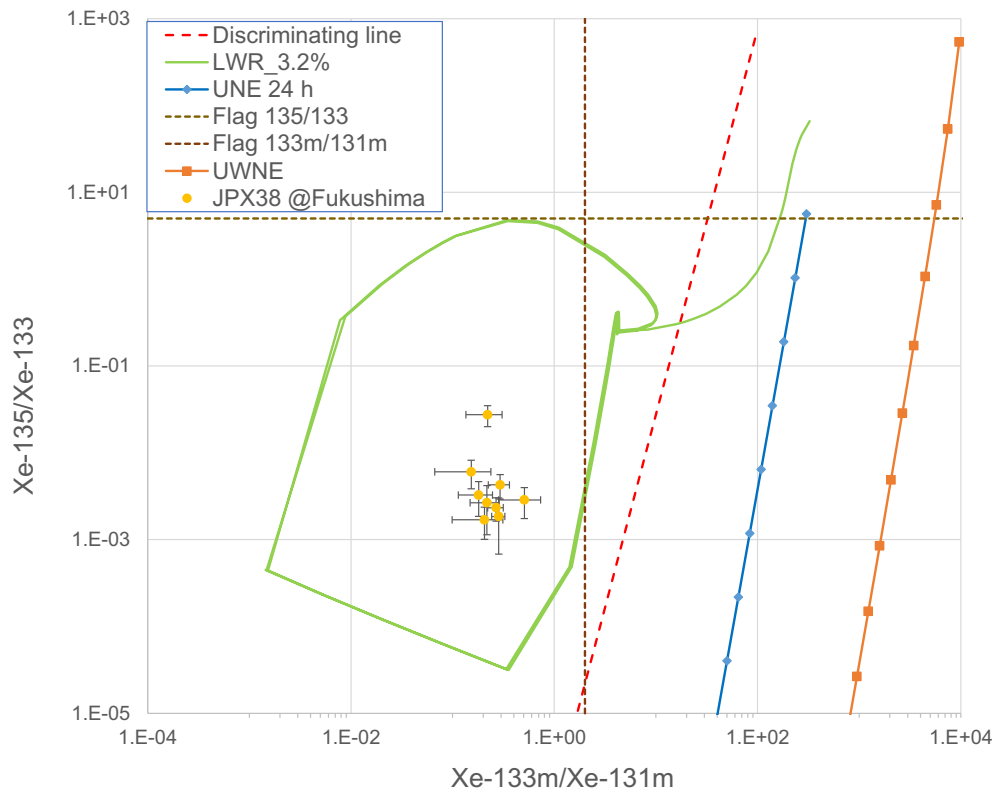


Figure 12

Four radioxenon plot of $^{135}\text{Xe}/^{133}\text{Xe}$ versus $^{133\text{m}}\text{Xe}/^{131\text{m}}\text{Xe}$. The evolution curves of the isotopic activity ratios for the two scenarios of ^{239}Pu are included: UNE release at 24 h after detonation and underwater nuclear explosion (UWNE) immediate release (Burnett et al., 2019). The uppermost point indicates the release at 24 h after the detonation time for UNE and zero hour for UWNE. The trajectory of LWR burn-up for 3.2% ^{235}U enrichment (evolution through three reactor circles) was replotted from Fig. 8 of Kalinowski et al. (2010). Four radioxenon isotopes were detected in a few samples at JPX38 after the Fukushima nuclear disaster in 2011 (Uncertainties of the isotopic activity ratios with two standard uncertainty)

6. Further Studies

6.1. Requirements of Isotopic Activity Ratio Analysis

The isotopic activity ratio analysis needs to combine the two ends of the source term and sample measurements for a possible match. A robust method is required that tests the isotopic activity ratios of samples against prepared information aggregated from a comprehensive set of all relevant release scenarios that could possibly explain the ratios detected at IMS radionuclide stations. Recent research results on the source mechanisms, including in-growth and decay, cavity-melt fractionation and seepage of cavity gases, are used to develop best-estimate input source terms as well as minimum and

maximum isotopic activity ratio boundaries as a function of time.

Libraries of scenarios for source term evolution are generated from the method coupling isotopic activity evolution of the gas-phase radioactive inventory to realistic physical models of cavity evolution. The input data will be aggregated to determine the envelope of isotopic activity ratios associated with UNEs. The output is a score for the consistency of the observations within the boundaries of all possible nuclear explosion signals.

In the applications related to IMS observations, this envelope can be constrained with the aid of available observational data. Estimates of the composition of prompt releases will be less affected by uncertainty in parameters controlling cavity-

evolution and gas leakage than late-time releases as represented by the DPRK2013 detection. Using isotopic analysis of the sample and related ATM simulations, the isotopic activity ratios at the source can be reconstructed as a function of time and geographic location. With additional information from waveform technologies this can be further constrained. For screening purposes, the reconstructed source ratios are compared with the envelope of possible isotopic activity ratios to provide a probabilistic estimate that the observations are associated with a UNE.

For characterization of a specific event, this comparison can be used to assist States Signatories in testing the hypothesis of an UNE being the source.

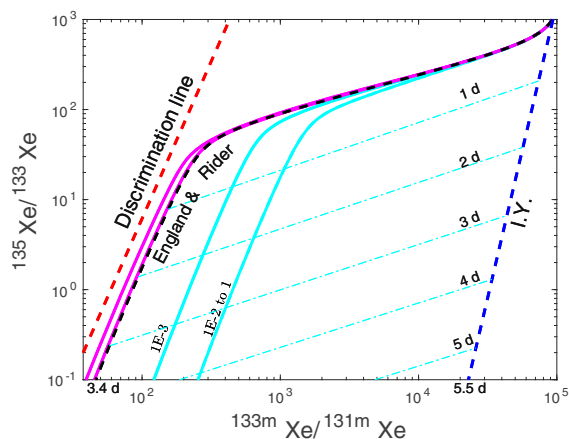


Figure 13

The standard 4-isotope plot shows the England & Rider-based model (black dashes) of radioxenon evolution assuming a well-mixed post-detonation cavity with no leakage of gases. A “discrimination line” (red dashes) lies to the left separating the E & R isotopic evolution model from most, if not all, atmospheric signals associated with civilian radionuclide sources (Kalinowski et al., 2010). Cyan-colored lines are two different isotopic evolution paths predicted by Carrigan et al. (2020) assuming different “rainout rates” of condensing refractory precursors of radioxenon into underlying molten rock with faster condensation and rainout moving the path to the right of the plot. Magenta-colored lines represent the evolutionary paths of radioxenon trapped in the underlying molten rock, which is a result of the rainout process and the initial partitioning of part of the radioactive inventory into the melt (Carrigan et al., 2020). Finally, the independent yield (I.Y.) (blue-dashed line) represents the evolutionary path of radioxenon isotopes produced at the time of detonation and before significant decay of precursors of radioxenon. Daily timelines are shown by the cyan-colored dot-dashed lines. Replotted from Fig. 5 of Carrigan et al. (2020)

6.2. Advanced Analysis Using Complicated Activity Evolution Models

In the case of detection of UNEs involving the observation of explosion-produced radionuclides in atmospheric air samples, radionuclide interference can come from sources such as medical isotope production facilities and commercial nuclear reactors (Saey & de Geer, 2005). Fortunately, comparing certain ratios of different radioxenon isotopes (131m , 133 , 133m , 135 Xe) due to commercial sources against values predicted by a radioactive-decay-chain model of post-detonation isotopic evolution indicates that many, if not all, civilian sources of atmospheric background can be distinguished from UNE sources by a “discrimination” line (Kalinowski et al., 2010) as illustrated in Fig. 12, and more scenarios in Fig. 13. The decay-chain model, mathematically represented by a version of the Bateman equation (Sun et al., 2015; Sloan et al., 2016), is based on the compilation of radioactive-decay data by England and Rider (1994) of those elements in the decay chain of a UNE. However, Carrigan et al. (2020) pointed out that this decay-chain model includes two assumptions that are not likely to be rigorously satisfied. The first requires refractory precursors (e.g., Sn, In, Sb, Te) to remain well mixed with gases including iodine and its radioxenon daughters during the evolution of the radionuclide inventory in the post-detonation cavity, while the second assumption requires gases not to leak from the cavity during the period of evolution.

6.3. Boundary Estimation Under Different Scenarios and Methods

Recently, the potential effects on the evolution of isotopic activity ratios of deviations from both assumptions (i.e., no leakage from the cavity and a well-mixed cavity) have begun to be explored. It has been known for decades from radiochemical studies of drill cores (e.g., Borg, 1975; Johnson & Violet, 1958) that a substantial portion of the post-detonation radioactive inventory is partitioned into a melt zone that forms at the bottom of the detonation cavity. The possibility that partitioning of the radioactive inventory or deviation from the well-mixed state might

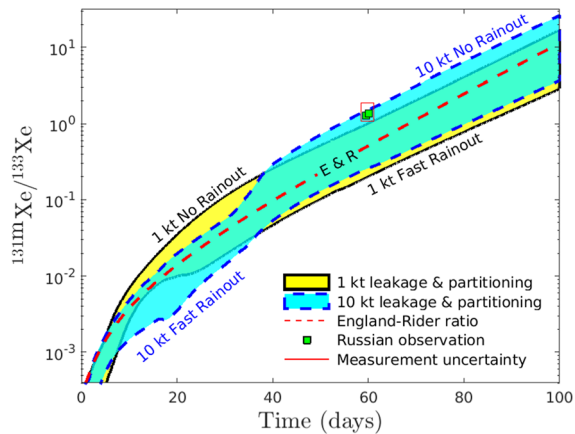


Figure 14

Evolution of the isotopic activity ratio $^{131\text{m}}\text{Xe}$ to ^{133}Xe in a detonation cavity is plotted against time for nuclear yields of 1 and 10 kt subject to assumed conditions of rainout and continuing loss of radionuclide inventory from the gas/vapor phase with leakage into the zone of containment. The idealized England and Rider model (i.e., full inventory remains well mixed with no long-term leakage from cavity) has been plotted (red dashed line) for comparison with the other cases. The rate of rainout or loss of refractory precursor inventory from the well-mixed state generally varies from the case of no rainout (system remains well-mixed) above the E & R line to rapid rainout below that line. The RUX58 measurements of the isotopic ratio resulting from the DPRK2013 event, which are interpreted as samples released from the cavity, are included for reference with the red box representing the estimated range of error for those measurements. While the curves presented are appropriate for a ^{235}U detonation, it is unknown what kind of fission event actually occurred. Cavity-gas seepage rates are only estimated for the DPRK2013 event. Replotted from Fig. 6 of Carrigan et al. (2020)

affect observable radioxenon activity ratios has been proposed by de Geer (2013) to interpret atmospheric radioxenon observations from DPRK UNEs. The exact nature of the process of partitioning or separation of refractory parents from radioxenon daughters is uncertain, but basic process models have been created and evaluated with the intent of estimating the impact of deviations from the well-mixed state (Carrigan et al., 2020). Figure 14 shows the effects of condensation and rainout of refractory parents during cooling of the gas phase followed by their capture in the melt zone of the detonation cavity. The main effect of partitioning by condensation and rainout of refractories is to shift the England & Rider evolutionary curve from its position near the discrimination line further to the right toward the independent yield (I.Y.) line. The extent of the

rightward shift depends on how quickly condensation and rainout can occur following detonation. For the example considered by Carrigan et al. (2020), the cyan lines show what happens when a condensing species has rainout half-life in the gas phase of approximately 700 s (label: 1.E-3) and 0.7 s (label: 1) (Fig. 13). To move any further rightward requires more rapid cooling to the starting point of precursor condensation. This result suggests that considering deviations from the assumption of a well-mixed radioactive inventory will generally increase the separation on the four radioxenon plot (Fig. 13) between atmospheric isotopic “noise” and the post-detonation radioxenon evolutionary curve.

It was found that relaxing the assumption of no leakage from the detonation cavity causes isotopic evolution to become dependent on nuclear yield through post-detonation heating and the resulting multiphase, thermally driven flow, which affects the time-dependent leakage rate (Sun and Carrigan, 2016; Carrigan et al., 2016). The DPRK2013 UNE was evaluated given evidence for long-term leakage from the cavity. Radionuclide observations of the nuclear test were unusual as radioxenon was not observed in the atmosphere until almost two months following the detonation with detections occurring first at JPX38 and a few days later at RUX58 (Ringbom et al., 2014). The measured ratios were somewhat different, leading to a possible interpretation by Ringbom and colleagues that the radioxenon measured first at JPX38, from what was evidently a well-contained UNE, was released in opening and ventilating the tunnel complex at the DPRK test site while the RUX58 observation, with large measurement errors (Ringbom et al., 2014), came from a location in the DPRK tunnel complex nearer to the point of detonation. Using their leaky reactor model in a variational study, Carrigan et al. (2016) reached a similar conclusion except that the RUX58 measurements were found to best agree with radioxenon evolution in the actual detonation cavity or chimney itself, for a yield of 5–8 kilotons, which happens to be in approximate agreement with the seismic yield estimates for that event (Oswald, 2013; Ringbom et al., 2014). This led to the hypothesis that the RUX58 measurements resulted from a prompt release caused by drilling back into the detonation cavity, a

common post-detonation procedure for nuclear test evaluation.

6.4. Radioxenon Background Estimation and Subtraction

One of the issues in the isotopic activity ratio analysis is whether the contribution of the radioxenon background needs to be subtracted. Simulations are performed with ATM to determine an activity concentration and its associated uncertainty from known releases of nuclear facilities to each IMS sample measurement, resulting in a residual between the IMS observation and ATM simulated concentration. Then, event discrimination can be performed based on the residual. However, there might be relatively large fluctuations in ATM simulated activity concentrations in some cases, resulting in outliers in the distributions of the residuals. In light of this issue, ATM simulations were performed to estimate the activity concentrations originating from hypothetical radioxenon releases of pre-defined UNEs as well as releases from known sources of nuclear facilities, resulting in synthetic activity concentrations at IMS stations. An ongoing study aims to get a better estimation of the radioxenon background to distinguish between known sources and potential (hidden or weaker) UNE signals. This will be done by exploring several methods that include statistical uncertainty for ATM simulated activity concentrations. Ultimately, the activity ratios of detected radioxenon isotopes are compared between the real IMS observations (typical radioxenon background), simulated concentrations from hypothetical nuclear explosion sources (pure signals without radioxenon background) and synthetic ones.

6.5. Data Fusion Between Radionuclide Observations and Waveform Events

The IMS network continuously monitors the globe for nuclear explosions through seismic, hydroacoustic, infrasound (SHI), and radionuclide measurements to detect signals from possible nuclear explosions. SHI monitoring stations continuously record waveform signals and the events identified using three technologies are fused into a combined

event bulletin. Due to the differing nature of SHI and radionuclide measurements, the results are reported in separate bulletins. In order to fully characterize a hypothetical UNE, the radionuclide detections must be matched to an event that was constructed from the waveform data of the SHI networks. The IDC regularly performs data fusion between radionuclide detections and waveform-based events using the source-receptor-sensitivity fields from the ATM simulations. In the scenarios considered here, a UNE creates an immediate seismic signal, but with an a-priori unknown time until the release of radionuclides. The data fusion pipeline at the IDC accounts for possible delayed releases of up to 60 days, but additional information is required to more precisely determine which waveform-based event should be associated with given radionuclide detections. The results described here, in particular the determination of the release (containment) time and the detonation time, can provide further information to the data fusion algorithm.

7. Conclusions

For both discrimination of a nuclear explosion source and estimation of the time of detonation, the first step is to estimate the isotopic activity ratio at the time of collection stop, which is based on activity concentrations in the plume of air. The isotopic ratio of two activity concentrations can be expressed by a non-linear model. Estimating the ratio value and associated uncertainty requires high-order Taylor expansion terms, such as the second-order polynomial. Therefore, the ratio and associated uncertainty are dependent not only on concentrations but also on their uncertainties and covariances. For isotopic activity ratio analysis, it would be more practical to use the MCM based on activities measured in the sample or associated peak counts in the spectrum analysis directly, especially for uncertainty estimation related to the elapsed time since the detonation time. The features of isotopic ratios of activities measured at the acquisition start time are different from the isotopic ratios of activities at the release time and activity concentrations in the plume of air at the time of collection stop. ATM connects the activity

evolution from the activity released at the explosion site through the activity concentration in the plume at IMS stations. The activity concentrations in the plume of air are used in isotopic activity ratio analysis for characterization of a nuclear release event. The event dating is based on a unique equation of the isotopic activity ratio with time under an assumed scenario. If the same decay chain is assumed in both before release and during atmospheric transport, the elapsed time can be estimated numerically by solving the Bateman equations. The uncertainty estimation can be performed using the MCM because of non-linear functions involved.

Characterization of radioxenon detections at IMS stations requires connecting or relating physical processes at the two ends of the lifetime of radioxenon isotopes and their isotopic activity ratios. The one end is the radioisotope generation by a nuclear explosion, the other end is their measurement in IMS samples. Mathematical modelling is used to explore the relationship between both ends, including ATM. Investigating IMS noble gas samples for possible nuclear test signatures requires all possible underground nuclear test scenarios to be tested.

Acknowledgements

The authors are grateful for constructive discussions and suggestions in the CTBT noble gas expert community in technical meetings while preparing this manuscript.

Author Contributions All authors contributed to the study conception and design. Material preparation, data collection and analysis were performed by BL, MK, CS, JW, YS, CRC, YK and RS. The first draft of the manuscript was written by BL, CRC and YS, and all authors commented on previous versions of the manuscript. All authors read and approved the final manuscript. (The views expressed in this paper are those of the authors and do not necessarily reflect the views of the CTBTO and LLNL that the authors represent.).

Funding

The authors declare that no funds, grants, or other support were received during the preparation of this manuscript.

Data availability

Nuclear fission yields and related data were taken from England and Rider (1994). The IMS measurement data and IDC analysis reports used in this paper would be available upon request.

Declarations

Conflict of interest The authors have no relevant financial or non-financial interests to disclose.

Open Access This article is licensed under a Creative Commons Attribution 4.0 International License, which permits use, sharing, adaptation, distribution and reproduction in any medium or format, as long as you give appropriate credit to the original author(s) and the source, provide a link to the Creative Commons licence, and indicate if changes were made. The images or other third party material in this article are included in the article's Creative Commons licence, unless indicated otherwise in a credit line to the material. If material is not included in the article's Creative Commons licence and your intended use is not permitted by statutory regulation or exceeds the permitted use, you will need to obtain permission directly from the copyright holder. To view a copy of this licence, visit <http://creativecommons.org/licenses/by/4.0/>.

Publisher's Note Springer Nature remains neutral with regard to jurisdictional claims in published maps and institutional affiliations.

REFERENCES

- Axelsson, A., & Ringbom, A. (2014). On the calculation of activity concentrations and nuclide ratios from measurements of atmospheric radioactivity. *Applied Radiation and Isotopes*, 92, 12–17.
- Bateman, H. (1910). The solution of a system of differential equations in the theory of radio-active transformation. *Proceedings of the Cambridge Philosophical Society*, 16, 423–427.
- Becker, A., Wotawa, G., De Geer, L., et al. (2007). Global backtracking of anthropogenic radionuclides by means of a receptor oriented ensemble dispersion modelling system in support of Nuclear-Test-Ban Treaty verification. *Atmospheric Environment*, 41, 4520–4534.
- Borg, I. Y. (1975). Radioactivity trapped in melt produced by a nuclear explosion. *Nuclear Technology*, 26(1), 88–100. <https://doi.org/10.13182/NT75-A24406>
- Burnett, J. L., Eslinger, P. W., & Milbrath, B. D. (2019). The detectability of the Wigwam underwater nuclear explosion by the radionuclide stations of the International Monitoring System. *Journal of Environmental Radioactivity*, 208–209, 106030.
- Carrigan, C., Sun, Y., Hunter, S. L., et al. (2016). Delayed signatures of underground nuclear explosions. *Scientific Reports*, 6, 1–9. <https://doi.org/10.1038/srep23032>

- Carrigan, C. R., Sun, Y., Pili, E., Neuville, D., & Antoun, T. (2020). Cavity-melt partitioning of refractory radionuclides and implications for detecting underground nuclear explosions. *Journal of Environmental Radioactivity*. <https://doi.org/10.1016/j.jenvrad.2020.106269>
- de Geer, L.-E. (2013). Reinforced evidence for a low-yield nuclear test in North Korea on 11 May 2010. *Journal of Radioanalytical and Nuclear Chemistry*, 298, 2075–2083.
- England, T.R., & Rider, B.F. (1994). Evaluation and compilation of fission product yields: 1993. Los Alamos report LA-UR-94e3106 (ENDF-349), Appendix A (Set A Yields evaluated and compiled), October 1994. ISO/IEC (2008).
- ISO 11929. (2019). Determination of the characteristic limits (decision threshold, detection limit and limits of the confidence interval) for measurements of ionizing radiation – fundamentals and application.
- ISO/IEC Guide 98-3. (2008). Uncertainty of measurement - Part 3: Guide to the expression of uncertainty in measurement, Supplement 1: Propagation of distributions using a Monte Carlo method.
- Johnson, G.W., & Violet, C.E. (1958). Phenomenology of contained nuclear explosions. University of California, Lawrence Radiation Laboratory, <https://doi.org/10.2172/4254880>, UCRL-5124 (Rev. 1).
- Kalinowski, M. B. (2011). Characterisation of prompt and delayed atmospheric radioactivity releases from underground nuclear tests at Nevada as a function of release time. *Journal of Environmental Radioactivity*, 102(9), 824–836. <https://doi.org/10.1016/j.jenvrad.2011.05.006>
- Kalinowski, M. B., Axelsson, A., Bean, M., et al. (2010). Discrimination of nuclear explosions against civilian sources based on atmospheric xenon isotopic activity ratios. *Pure and Applied Geophysics*, 167(4–5), 517–539. <https://doi.org/10.1007/s00024-009-0032-1>
- Kalinowski, M.B. & Liu, B. (2020). Calculation of isotopic ratios of fission products detected at IMS radionuclide stations. Proceedings of the INMM 61st Annual Meeting July 12–16, 2020, Baltimore, MD, USA.
- Kalinowski, M. B., & Pistner, C. (2006). Isotopic signature of atmospheric xenon released from light water reactors. *Journal of Environmental Radioactivity*, 88(3), 215–235. <https://doi.org/10.1016/j.jenvrad.2006.02.003>
- Kijima Y., Kalinowski, M.B, Liu, B. et al. (2022). Investigation on sample association by using anomalous concentration episodes and decay-consistent isotopic ratios at IMS radionuclide stations. Proceedings of the INMM 63rd Annual Meeting July 24–28, 2022.
- Kuśmierczyk-Michulec, J., Becker, A., Wotawa, G. et al. (2021). Advancements in Atmospheric Transport Modelling (ATM) at the CTBTO PTS during the past two decades and plans for the future, CTBT Science and Technology Conference 2021 (SnT2021), <https://conferences.ctbto.org/event/7/contributions/1367/>.
- Liu, B. & Kalinowski, M.B. (2021). Estimation of isotopic ratios of fission products by using the Monte-Carlo method. Proceedings of the INMM & ESARDA Joint Virtual Annual Meeting August 23–26 & August 30–September 1, 2021.
- MathWorks. (2000). *MATLAB high-performance numeric computation and visualization software*, Web site: www.mathworks.com, Natick, MA, USA.
- Oswald, R. (2013). North Korean nuclear test more than twice as powerful as last blast. In *Global security newswire*. (Date of access:16/12/2015).
- Ringbom, A., Axelsson, A., Aldener, M., et al. (2014). Radioxenon detections in the CTBT international monitoring system likely related to the announced nuclear test in North Korea on February 12, 2013. *Journal of Environmental Radioactivity*, 128, 47–63.
- Saey, P. R. J., & De Geer, L.-E. (2005). Notes on radioxenon measurements for CTBT verification purposes. *Applied Radiation and Isotopes*, 63, 765–773.
- Schwartz, L., Piwinskii, A., Ryerson, F., Tewes, H., & Beiriger, W. (1984). Glass produced by underground nuclear explosions. *Journal of Non-Crystalline Solids*, 67(1–3), 559–591.
- Sloan, J., Sun, Y., & Carrigan, C. (2016). Uncertainty quantification for discrimination of nuclear events as violations of the comprehensive nuclear-test-ban treaty. *Journal of Environmental Radioactivity*, 155, 130–139.
- Stohl, A., Forster, C., Frank, A., Seibert, P., & Wotawa, G. (2005). Technical Note: The Lagrangian particle dispersion model FLEXPART version 6.2. *Atmospheric Chemistry and Physics*, 5, 2461–2474. <https://doi.org/10.5194/acp-5-2461-2005>
- Stohl, A., Hittenberger, M., & Wotawa, G. (1998). Validation of the Lagrangian particle dispersion model FLEXPART against large scale tracer experiments. *Atmospheric Environment*, 32, 4245–4264.
- Stohl, A., & Thomson, D. J. (1999). A density correction for Lagrangian particle dispersion models. *Boundary-Layer Meteorology*, 90, 155–167.
- Sun, Y., & Carrigan, C. R. (2016). Thermally driven advection for radioxenon transport from an underground nuclear explosion. *Geophysical Research Letters*, 43, 4418–4425. <https://doi.org/10.1002/2016GL068290>
- Sun, Y., Carrigan, C., Cassata, W., Hao, Y., Ezzedine, S., & Antoun, T. (2021). A closed-form solution for source-term emission of xenon isotopes from underground nuclear explosions. *Transport in Porous Media*, 139, 131–153. <https://doi.org/10.1007/s11242-021-01650-x>
- Sun, Y., Carrigan, C. R., & Hao, Y. (2015). Radioxenon production and transport from an underground nuclear detonation to ground surface. *Pure and Applied Geophysics*, 172, 243–265.
- Wotawa, G., De Geer, L., Denier, P., et al. (2003). Atmospheric transport modelling in support of CTBT verification-Overview and basic concepts. *Atmospheric Environment*, 37, 2529–2537.
- Yamba, K., Sanogo, O., Kalinowski, M. B., Nikkinen, M., & Koulidiati, J. (2016). Fast and accurate dating of nuclear events using La-140/Ba-140 isotopic activity ratio. *Applied Radiation and Isotopes*, 112, 141–146.
- Zaehring, M., & Kirchner, G. (2008). Nuclide ratios and source identification from high-resolution gamma-ray spectra with Bayesian decision methods. *Nuclear Instruments and Methods in Physics Research Section a: Accelerators, Spectrometers, Detectors and Associated Equipment*, 594(3), 400–406.